

Determination of Landé g_J factor and Zeeman coefficients in ground-state $^{171}\text{Yb}^+$ and their applications to quantum frequency standards

Jize Han,^{1,2} Benquan Lu,³ Yanmei Yu,^{4,5,*} Jiguang Li,^{6,†} Zhiguo Huang,² Jingwei Wen,² Ling Qian,^{2,‡} and Lijun Wang^{1,7,§}

¹*State Key Laboratory of Precision Measurement Technology and Instruments, Department of Precision Instrument, Tsinghua University, Beijing 100084, China*

²*China Mobile (Suzhou) Software Technology Company Limited, Suzhou 215163, China*

³*National Time Service Center, Chinese Academy of Sciences, Xi'an 710600, China*

⁴*Beijing National Laboratory for Condensed Matter Physics, Institute of Physics, Chinese Academy of Sciences, Beijing 100190, China*

⁵*University of Chinese Academy of Sciences, Beijing 100049, China*

⁶*Institute of Applied Physics and Computational Mathematics, Beijing 100088, China*

⁷*Department of Physics, Tsinghua University, Beijing 100084, China*

(Dated: January 20, 2025)

We report the determination of the Landé g_J factor and Zeeman coefficients for the ground-state of $^{171}\text{Yb}^+$, relevant to microwave quantum frequency standards (QFSs). The g_J factor is obtained by using two independent methods: multiconfiguration Dirac-Hartree-Fock and multireference configuration interaction, yielding a consistent value of 2.002615(70). The first- and second-order Zeeman coefficients are determined as 14,010.78(49) Hz/ μT and 31.0869(22) mHz/ μT^2 , respectively, based on the calculated g_J factor. These coefficients enable reduced magnetic-field-induced uncertainties, improving the accuracy of the $^{171}\text{Yb}^+$ microwave QFSs. The results reported in this work also offer potential for improved constraints on variations in fundamental constants through frequency comparisons, and advancing trapped-ion quantum computers based on the ground-state hyperfine splitting of $^{171}\text{Yb}^+$.

I. INTRODUCTION

Microwave quantum frequency standards (QFSs) are among the most widely utilized quantum technologies, offering critical applications in timekeeping and precision measurements. Trapped-ion microwave QFSs represent the next generation of this technology, providing superior stability, precision, and portability [1]. Among the various trapped-ion systems, $^{171}\text{Yb}^+$ stands out as particularly advantageous compared to other ions such as $^{199}\text{Hg}^+$ [2, 3] and $^{113}\text{Cd}^+$ [4–11]. This advantage arises from its fiber-friendly cooling and repumping laser wavelengths, which can be generated using compact semiconductor lasers. These unique features make $^{171}\text{Yb}^+$ an attractive candidate for developing compact and practical microwave QFSs [12–19].

In microwave QFSs based on laser-cooled trapped ions, all external fields are minimized except for the magnetic field, which is essential to provide a quantization axis for the ions. This field, commonly referred to as the “C-field” in the QFS community, introduces the most significant frequency shift in trapped-ion microwave QFSs: the second-order Zeeman shift (SOZS). For example, the SOZS contributes over 99% of the total systematic shifts in laser-cooled Cd^+ [11, 20] and Yb^+ [13, 21] microwave QFSs. In laser-cooled Hg^+ microwave QFSs, even with

only five ions and liquid helium cooling to reduce the required C-field at the cost of stability and portability, the SOZS still accounts for approximately 97% of the total systematic shifts [2]. Therefore, a rigorous evaluation of the magnitude and uncertainty of the SOZS is crucial.

Accurate determination of the SOZS requires precise knowledge of the first- and second-order Zeeman coefficients, K_Z and K_0 . These coefficients can be determined using extrapolation methods in experiments [22–25]. Additionally, deriving K_Z and K_0 from the g_J factor provides reliable data and serves as a benchmark for extrapolation techniques [22–25]. Since g'_I [26] and A [13] have been determined with high accuracy, the values of K_Z and K_0 primarily depend on the precise determination of the electronic g_J factor. Experimental spectroscopic measurements yield $g_J = 1.998$ [27], while theoretical calculations provide varying predictions: the relativistic coupled-cluster (RCC) method estimates $g_J = 2.002798(113)$ [28], and the time-dependent Hartree-Fock (TDHF) method gives $g_J = 2.003117$ [29]. Although these theoretical values are in general agreement, they differ by approximately 0.0003. Under typical magnetic field strengths (3–10 μT) [2, 11, 13, 19], this discrepancy in g_J leads to a fractional uncertainty in the SOZS of $(0.8\text{--}7.9) \times 10^{-14}$. Such uncertainty does not meet the accuracy requirements for state-of-the-art $^{171}\text{Yb}^+$ microwave QFSs [13, 19, 30].

Beyond QFS applications, the level structure of $^{171}\text{Yb}^+$ makes it an excellent candidate for testing the Standard Model and exploring potential new physics. This ion features two optical clock transitions: the E2 transition at 436 nm and the E3 transition at 467 nm.

* ymyu@aphy.iphy.ac.cn

† li_jiguang@iapcm.ac.cn

‡ qianling@cmss.chinamobile.com

§ lwan@mail.tsinghua.edu.cn

Frequency comparisons between these transitions have established the most stringent constraints to date on the temporal variation of the fine-structure constant α , reaching a level of 10^{-19} [24, 31, 32]. Additionally, $^{171}\text{Yb}^+$ exhibits a 12.6-GHz hyperfine splitting (HFS) that is sensitive to variations in the quark mass to strong-interaction scale ratio, m_q/Λ_{QCD} ($^{171}\text{Yb}^+$: -0.099 vs ^{133}Cs : 0.002) [33, 34]. The prospect of conducting frequency comparisons between the two optical clock transitions and the microwave clock transitions of $^{171}\text{Yb}^+$ within a unified experimental setup is particularly promising. This approach mitigates various common-mode frequency shift uncertainties, including those arising from pressure, gravitational effects, black-body radiation, frequency synchronization, and detection noise, thereby extending the application of the $^{171}\text{Yb}^+$ microwave QFSs in testing variations of fundamental constants. Moreover, the 12.6-GHz ground-state HFS of $^{171}\text{Yb}^+$ also encodes as a Qubit level in trapped-ion quantum computers [35–38]. Thus, improving the accuracy of the Yb^+ g_J factor and, consequently, the accuracy of HFS evaluations, could support constraints on the variation of fundamental constants through microwave-optical frequency comparisons and advancements in trapped-ion quantum computers.

In this work, we present the determination of the ground-state Landé g_J factor and Zeeman coefficients in $^{171}\text{Yb}^+$ for microwave QFS applications. To achieve an accurate g_J factor, we employ two independent theoretical methods: multiconfiguration Dirac-Hartree-Fock (MCDHF) and multireference configuration interaction (MRCI). These methods yield a consistent value of $g_J = 2.002615(70)$. Based on this result, we derive the first- and second-order Zeeman coefficients as 14,010.78(49) Hz/ μT and 31.0869(22) mHz/ μT^2 , respectively. This work improves the accuracy in evaluating the ground-state HFS of $^{171}\text{Yb}^+$, thereby supporting its applications in microwave QFSs, fundamental constant variation constraints, and trapped-ion quantum computers.

II. THEORY AND METHODS

In the $6s\ ^2S_{1/2}$ ($F = 0, m_F = 0$) \rightarrow ($F = 1, m_F = 0$) HFS of $^{171}\text{Yb}^+$, the SOZS in a weak magnetic field regime ($B_0 < A/\mu_B$) can be described as [39],

$$\Delta\nu_{\text{SOZS}} = K_0 B_0^2 = K_0 \left(\frac{\Delta\nu_L}{2K_Z}\right)^2, \quad (1)$$

where

$$K_0 = \frac{(g_J - g'_I)^2 \mu_B^2}{2h^2 A}, \quad (2)$$

represents the SOZS coefficient, g_J and g'_I are the electronic and nuclear g factors, μ_B and h corresponds to the Bohr magneton and the Planck constant, A denotes the

ground-state hyperfine constant; and

$$K_Z = \frac{(g_J + g'_I)\mu_B}{2h}, \quad (3)$$

represents the first-order Zeeman coefficient. By incorporating the Larmor frequency difference, $\Delta\nu_L$, between the Zeeman sublevels $6s\ ^2S_{1/2}$ ($F = 0, m_F = 0$) \rightarrow ($F = 1, m_F = \pm 1$), we can calibrate the static magnetic field, B_0 , experienced by the ions.

The interaction Hamiltonian between an atom and the magnetic field can be written as [40]

$$H_m = (\mathbf{N}^{(1)} + \Delta\mathbf{N}^{(1)}) \cdot \mathbf{B}, \quad (4)$$

by choosing the direction of the magnetic field as the z -direction and neglecting all diamagnetic contributions in a relativistic frame. The electronic tensor operators of an N -electron atom can be expressed as [41],

$$\begin{aligned} \mathbf{N}^{(1)} &= \sum_{i=1}^N \mathbf{n}^{(1)}(i) = \sum_{i=1}^N -i \frac{\sqrt{2}}{2\alpha} r_i (\boldsymbol{\alpha}_i \mathbf{C}^{(1)}(i))^{(1)}, \\ \Delta\mathbf{N}^{(1)} &= \sum_{i=1}^N \Delta\mathbf{n}^{(1)}(i) = \sum_{i=1}^N \frac{g_s - 2}{2} \beta_i \boldsymbol{\Sigma}_i, \end{aligned} \quad (5)$$

where $\boldsymbol{\Sigma}_i$ represents the relativistic spin matrix, i denotes the imaginary unit, and the term $\Delta\mathbf{N}^{(1)}$ corresponds to the Schwinger QED correction. The $g_s = 2.00232$ is the electron spin g_J factor, which is adjusted by a factor of 1.001160 to account for quantum electrodynamics (QED) effects. The uncertainty in g_s is significantly smaller than the current many-body calculation accuracy and therefore can be negligible. The interaction Hamiltonian H_m can be treated in first-order perturbation theory in a weak magnetic field situation. The g_J factor is defined as

$$g_J = 2 \frac{\langle \Gamma P M_J J | | \mathbf{N}^{(1)} + \Delta\mathbf{N}^{(1)} | | \Gamma P M_J J \rangle}{\sqrt{J(J+1)}}, \quad (6)$$

where P is the parity, J is total angular momentum, M_J is the component along the z direction of J , Γ represents another appropriate angular momentum, and $|\Gamma J P M_J\rangle$ is the atomic state function (ASF) which can be obtained using the MCDHF and MRCI methods.

A. The MCDHF method

The MCDHF method [42] is implemented in the GRASP package [43]. The ASF in the MCDHF method are approximate eigenfunctions of the Dirac-Coulomb-Breit Hamiltonian describing an atomic system,

$$\begin{aligned} H_{\text{DCB}} &= \sum_i [c \boldsymbol{\alpha}_i \cdot \mathbf{p}_i + (\beta_i - 1)c^2 + V_{\text{nuc}}(r_i)] + \sum_{i < j}^N \frac{1}{r_{ij}} \\ &\quad - \frac{1}{2r_{ij}} \left[\boldsymbol{\alpha}_i \cdot \boldsymbol{\alpha}_j + \frac{(\boldsymbol{\alpha}_i \cdot \mathbf{r}_{ij})(\boldsymbol{\alpha}_j \cdot \mathbf{r}_{ij})}{r_{ij}^2} \right], \end{aligned} \quad (7)$$

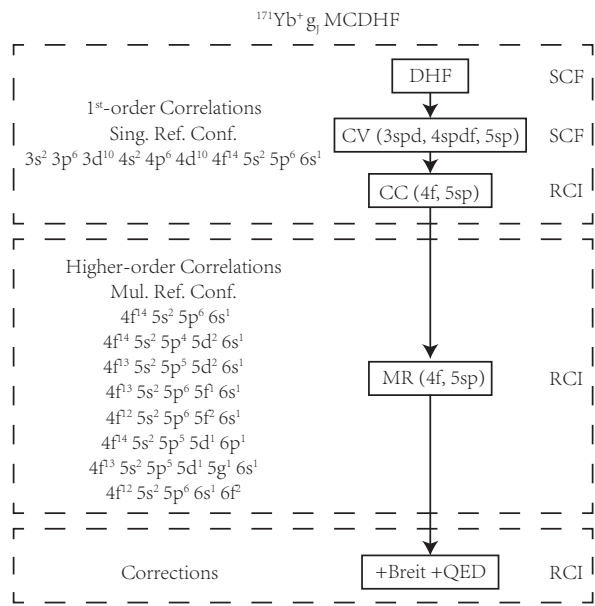


FIG. 1. The computational model employed in the MCDHF method incorporates both first-order and higher-order electron correlations. The first-order electron correlations encompass the CV and CC correlations. The higher-order electron correlations are considered by the MR-SD method. Corrections for the Breit interaction and QED effects are included in the final model.

where α and β represent the Dirac matrices, \mathbf{p}_i is the momentum operator, r_{ij} is the distance between electrons i and j , and $V_{\text{nuc}}(r)$ is the nuclear potential results from a nuclear charge density given by a two-parameter Fermi distribution function [44]. The last term is the Breit interaction in the low-frequency approximation. The ASF is a linear combination of configuration state functions (CSFs) [45],

$$|\Gamma P J M_J\rangle = \sum_{i=1}^{N_{\text{CSF}}} c_i |\Gamma_i P J M_J\rangle. \quad (8)$$

where c_i are the expansion (mixing) coefficients. The CSFs are the linear combinations of one-electron Dirac orbital products.

The active set approach is employed to generate CSFs, with the selection of CSFs determining the electron correlation effects to be considered. The computational model is outlined in Fig. 1. The calculations begin with the Dirac-Hartree-Fock (DHF) approximation, optimizing the occupied spectroscopic orbitals for the reference configuration $\{[\text{Ne}]3s^2 3p^6 3d^{10} 4s^2 4p^6 4d^{10} 4f^{14} 5s^2 5p^6 6s\}$. In this configuration, the outermost $6s$ orbital is treated as valence electron, while the remaining orbitals are considered core electrons. Valence-core ($n \geq 3$) correlations (CV) are included in the self-consistent field (SCF) calculations, labeled as ‘‘CV’’ in Table I. These correlations are accounted for using single and restricted double (SrD) substitutions from the $n \geq 3$ core orbitals, where only one

electron in the core orbital is allowed to be excited to the correlation orbitals. The correlation orbitals are systematically expanded to $\{14s, 13p, 12d, 12f, 10g, 10h, 8i\}$, with only the latest added orbitals optimized in each step. Core-core (CC) correlations are considered in the relativistic configuration interaction (RCI) calculations, where only the mixing coefficients are varied. The CC correlations are incorporated using CSFs generated via single and double (SD) substitutions from the $4f^{14} 5s^2 5p^6 6s$ core orbitals to the largest correlation orbitals, as indicated by ‘‘CC’’ in Table I.

Higher-order electron correlations in the MCDHF calculations are efficiently incorporated through SD excitations from multi-reference (MR) configurations [46, 47]. In this approach, CSFs with significant mixing coefficients from the first-order correlations are selected to construct the MR configuration set. SD excitations from this MR configuration set capture the dominant higher-order electron correlation effects. Initially, configurations $\{4f^{14} 5s^2 5p^4 5d^2 6s; 4f^{13} 5s^2 5p^5 5d^2 6s\}$, with mixing coefficients greater than 0.03, are included and labeled as ‘‘MR-I’’. Subsequently, configurations $\{4f^{13} 5s^2 5p^6 5f^1 6s; 4f^{12} 5s^2 5p^6 5f^2 6s; 4f^{14} 5s^2 5p^5 5d^1 6p; 4f^{13} 5s^2 5p^5 5d^1 5g^1 6s; 4f^{12} 5s^2 5p^6 6s 6f^2\}$, with mixing coefficients between 0.025 and 0.03, are added and referred to as ‘‘MR-II’’. In the MR model, only two layers of correlation orbitals are utilized to generate CSFs due to their rapid convergence. These configurations are incorporated into the ‘‘CC’’ calculation for the reference configuration, as summarized in Table I. Finally, Breit interaction and QED effects (vacuum polarization and self-energy) are included within the RCI procedure in the MR-II model.

The g_J factors obtained from different computational models based on the MCDHF method are presented in Table I. The CV correlation is the dominant effect, while the CC correlation and higher-order correlations exhibit a canceling effect, consistent with previous observations in the HFS [47]. Incorporating the primary CV, CC, and higher-order correlations yields a g_J of 2.002635 from the MCDHF calculations. Breit interaction and QED effects contribute corrections of approximately -0.000010 and 0.000001 , respectively, refining the g_J to 2.002626.

A comprehensive evaluation of the upper and lower bounds of the g_J using the MCDHF method is conducted to quantify the calculation uncertainty. The calculated g_J exhibits an increasing trend with the MR configurations expansion. The upper bound of the g_J , constrained by the convergence of the MR expansion, is estimated to be less than the difference between the g_J values obtained from the MR-II and MR-I configurations, which is 0.000057. Electron correlations from the $n = 1, 2, 3$ shells and the $4s$, $4p$, and $4d$ orbitals, could reduce the g_J . Contributions of the CC and higher-order correlations from the $4f$, $5s$, and $5p$ orbitals are calculated as -0.000356 and 0.000107 , respectively, as shown in Table 1, indicating a cancellation effect of at least 30%. The CC contributions from the $4s$, $4p$, and $4d$ orbitals are

TABLE I. The MCDHF calculations of g_J factors using different levels of modeling. NCSF denotes the number of configuration state functions for each model.

Model	Reference configurations	Correlation orbitals	NCSF	g_J
DHF	$\{5s^25p^66s\}$	$\{5s,5p,6s\}$	1	2.002240
CV	$\{3s^23p^63d^{10}4s^24p^64d^{10}4f^{14}5s^25p^66s\}$	$\{14s,13p,12d,12f,10g,10h,8i\}$	25618	2.002884
CC	$\{4f^{14}5s^25p^66s\}$	$\{14s,13p,12d,12f,10g,10h,8i\}$	170109	2.002528
MR-I	$\cup\{4f^{14}5s^25p^45d^26s; 4f^{13}5s^25p^55d^26s\}$	$\{8s,7p,7d,6f,6g,6h\}$	851089	2.002578
MR-II	$\cup\{4f^{13}5s^25p^65f^16s; 4f^{12}5s^25p^65f^26s;$ $4f^{14}5s^25p^55d^16p; 4f^{13}5s^25p^55d^15g^16s;$ $4f^{12}5s^25p^66s6f^2\}$	$\{8s,8p,7d,8f,6g,6h\}$	2654356	2.002635
Final				2.002626
Uncertainty				0.000057

calculated to be -0.000076 . Considering the cancellation effect, the lower bound of the g_J due to CC and higher-order electron correlations among electrons with $n \leq 4d$ is estimated to be less than -0.000057 . Other sources of uncertainty are within this range. Consequently, the g_J derived from the MCDHF calculations is determined to be 2.002626(57), where the value in parentheses represents the estimated uncertainty.

B. The MRCI method

The MRCI method is implemented within the KR-CI module of the DIRAC package [48, 49]. The computational procedure begins with a closed-shell DHF calculation of Yb^{2+} using the Dirac-Coulomb-Gaunt Hamiltonian. This Hamiltonian is expressed as

$$H_{\text{DCG}} = \sum_i [c \boldsymbol{\alpha}_i \cdot \mathbf{p}_i + (\beta_i - 1)c^2 + V_{\text{nuc}}(r_i)] + \sum_{i < j} \left[\frac{1}{r_{ij}} - \frac{\boldsymbol{\alpha}_i \cdot \boldsymbol{\alpha}_j}{2r_{ij}} \right]. \quad (9)$$

The last term in Eq. (9) corresponds to the Gaunt interaction, which constitutes the primary component of the Breit interaction. The Gaunt interaction is only included in the DHF calculation. We have employed Dyall's core-valence triple-zeta and quadruple-zeta basis sets, which have $30s, 24p, 16d, 11f, 3g, 2h$ functions (dyall.cv3z) and $35s, 30p, 19d, 13f, 5g, 4h, 2i$ functions (dyall.cv4z) [50]. We have also used the doubly diffusion augmented basis set of dyall.cv4z, as denoted by 'd-aug-dyall.cv4z'. Besides, we have carried out the densification in the $s, p, d, f,$ and g spaces of the dyall.cv4z basis by using the technique way suggested in Ref. [51], which increase the basis size up to $69s, 59p, 37d, 25f, 9g, 4h,$ and $2i$ functions.

The MRCI calculation is performed after the DHF calculation. The MRCI method is based on the general active space (GAS) concept [52–54]. Through defining the minimum (Min.) and maximum (Max.) numbers of the accumulated electron occupation, the number (#) of the

Kramer pair, and the allowed excitation ranks that can be single (S), the single and double (SD), and the single, double, and triple (SDT), we choose four different CI wave-function models that are illustrated in Table II. Firstly, we take the outmost 23 electrons into account, which includes the $5s^25p^64f^{14}$ core and the $6s$ valence electron, as labeled by 'e23-SD'. Then we add the $4d$ core, which leads to a model with the outmost 33 electrons, as labeled by 'e33-SD'. Next, the allowed excitation ranks are increased to bring the triple electronic correlations, which are labeled by 'e23-SDT-I(II)'. The remaining unoccupied spinors consist of the virtual subspace. The high-lying virtual orbitals with energy larger than m a.u. as denoted by ' $< m$ ', are truncated, which is tested to ensure the convergence of the results with such operation.

The value of g_J obtained using different GAS models are summarized in Table III. First of all, the 'e23-SD' and 'e33-SD' models are implemented with the dyall.cv3z, dyall.cv4z, diffusion augmented and *spdfg*-densified dyall.cv4z basis sets. All of these calculations have shown the excellent convergence of the obtained g_J values with the increasing basis sets as well as inclusion of more inner core and virtual spinors. However, the results using the 'e23-SDT' model shows great changes, which indicates the important role of the triple excitation to the g_J value. The 'e23-SDT-I' <10 calculation with the dyall.cv4z basis set obtains $g_J = 2.002604$. The result of the 'e23-SDT-II' <10 calculation, which adds SD excitation arising from the $5s^25p^6$ shells, is consistent with the 'e23-SDT-I' <10 calculation with the same basis set. Repeating the 'e23-SDT-I' <10 calculation with the d-aug-dyall.cv4z basis set shows the fluctuation of the g_J values around 0.000055. Therefore, we take the g_J value obtained by the 'e23-SDT-I' <10 calculation with the dyall.cv4z basis set as the final value, while taking the difference between that and one with the d-aug-dyall.cv4z basis set as the uncertainty. To check the dependence of the calculation results on the DHF reference state, we have also conducted the 'e23-SD' <5 calculation with the dyall.cv3z basis set and the 'e23-SDT-I' <10 calculation with the dyall.cv4z basis set that are based on the $\text{Yb}^+ 6s_{1/2}$ open-shell DHF calculation. These calcula-

TABLE II. The general active space model in the MRCI calculations.

Model	Min.	Max.	# of Kramer pair	Function type	Excitation rank
e23-SD	7	8	4	$5s^25p^6$, core	S
	21	22	7	$4f^{14}$, core	S
	21	23	1	6s, valence	SD
	23	23	m	virtual	
e33-SD	9	10	5	4d, core	S
	17	18	4	$5s^25p^6$, core	S
	31	32	7	$4f^{14}$, core	S
	31	33	1	6s, valence	SD
	33	33	m	virtual	
e23-SDT-I	7	8	4	$5s^25p^6$, core	S
	20	22	7	$4f^{14}$, core	SD
	20	23	1	6s, valence	SDT
	23	23	m	virtual	
e23-SDT-II	6	8	4	$5s^25p^6$, core	SD
	20	22	7	$4f^{14}$, core	SD
	20	23	1	6s, valence	SDT
	23	23	m	virtual	

TABLE III. The MRCI calculations of g_J performed at different levels of modeling.

Index	Model	Basis	NCSF	active virtual spinors	g_J
(1)	e23-SD < 5	dyall.cv3z	34163	{10s, 10p, 8d, 7f, 5g, 6h}	2.002857
(2)	e23-SD < 5 *	dyall.cv3z	34163	{10s, 10p, 8d, 7f, 5g, 6h}	2.002850
(3)	e33-SD < 5	dyall.cv3z	50155	{10s, 10p, 8d, 7f, 5g, 6h}	2.002868
(4)	e23-SD < 10	dyall.cv4z	96626	{12s, 12p, 9d, 9f, 7g, 7h, 7i}	2.002863
(5)	e23-SD < 15	dyall.cv4z	113980	{13s, 13p, 10d, 9f, 7g, 7h, 7i}	2.002855
(6)	e23-SD < 50	dyall.cv4z	210214	{14s, 14p, 11d, 11f, 8g, 8h, 8i}	2.002862
(7)	e23-SD < 10	d-aug-dyall.cv4z	232734	{14s, 14p, 11d, 11f, 9g, 9h, 9i}	2.002852
(8)	e23-SD < 10	densified-dyall.cv4z	235168	{14s, 14p, 11d, 11f, 9g, 9h, 8i}	2.002855
(9)	e23-SDT-I < 10	dyall.cv4z	37446858	{12s, 12p, 9d, 9f, 7g, 7h, 7i}	2.002604
(10)	e23-SDT-I < 10 *	dyall.cv4z	37446858	{12s, 12p, 9d, 9f, 7g, 7h, 7i}	2.002636
(11)	e23-SDT-II < 10	dyall.cv4z	86600398	{12s, 12p, 9d, 9f, 7g, 7h, 7i}	2.002585
(12)	e23-SDT-I < 10	d-aug-dyall.cv4z	262470976	{14s, 14p, 11d, 11f, 9g, 9h, 9i}	2.002659
	Final				2.002604
	Uncertainty				0.000055

tions are marked by ‘*’ in Table III. Their results show that the variation of the g_J due to difference of DHF reference spinors is within the margin of our estimation to the uncertainty. Therefore, the g_J in the MRCI calculation is determined to be 2.002604(55), where the number in parentheses indicates the uncertainty.

III. RESULTS AND DISCUSSIONS

The g_J factor, along with the first- and second-order Zeeman coefficients of the $^{171}\text{Yb}^+$ ground-state determined in this work, are presented in Table IV, with uncertainties provided in parentheses. Our MCDHF and MRCI calculations yield $g_J = 2.002626(57)$ and

$g_J = 2.002604(55)$, respectively. Note that these are two independent, back-to-back calculations, with no computational parameters adjusted to align the two results. Based on the mean value of the MCDHF and MRCI calculated results, we determined $g_J = 2.002615(70)$, with the value in parentheses representing the upper bound of the uncertainty, covering the uncertainty budgets of both the MCDHF and MRCI calculations [56–58]. Another method for evaluating uncertainty based on the weighted mean is presented in the appendix.

The final result, $g_J = 2.002615(70)$, lies near the lower bound of the previously RCC value, $g_J = 2.002798(113)$ [28], while improving the consistency of the Landé g_J factor to the fifth decimal place, as shown in Table IV. The TDHF method yields $g_J = 2.003117$ [29], which is larger

TABLE IV. The g_J factors, first-order Zeeman coefficients (K_Z , in Hz/ μ T), and second-order Zeeman coefficients (K_0 , in mHz/ μ T²) for the ground-state $^{171}\text{Yb}^+$. Results from previous studies are included for comparison. Abbreviations: MCDHF, multiconfiguration Dirac-Hartree-Fock; MRCl, multireference configuration interaction; RCC, relativistic coupled-cluster; TDHF, time-dependent Hartree-Fock; Nonrel., nonrelativistic; Spectr., spectroscopic measurement.

g_J factor			
g_J		Source	Type
2.002626(57)		MCDHF	Theor.
2.002604(55)		MRCl	Theor.
2.002615(70)		Final	Theor.
2.002798(113)		RCC [28]	Theor.
2.003117		TDHF [29]	Theor.
2.0023		Nonrel. [55]	Theor.
1.998		Spectr. [27]	Exp.
Zeeman coefficients			
K_Z	K_0	Source	Type
14,010.78(49)	31.0869(22)	Final	Theor.
14,008.6	31.077	Nonrel. [55]	Theor.
14,012.06(79) ^a	31.0926(35) ^a	RCC [28] ^a	Theor.
14,014.30 ^a	31.1025 ^a	TDHF [29] ^a	Theor.
13,980 ^a	30.9 ^a	Spectr. [27] ^a	Exp.

^aDerived by using g_J provided in each Refs.

than our final result as well as others. The only available experimental result, $g_J = 1.998$, comes from an early spectroscopic measurement with only four effective digits and no reported uncertainty [27], and is substantially lower than our result as well as others. This discrepancy highlights the necessity for further measurements. Accurate calculations of the Landé g_J factor remain challenging, even for alkali-metal atoms and alkali-metal-like ions [59], due to their sensitivity to electron correlation effects. These challenges are further compounded in Yb^+ by the complexities associated with $4f$ -orbital electrons, which have been shown to be both significant and intricate [60]. Thus, the results presented in this work could provide valuable insights into the electron correlation effects contributing to the Landé g_J factor of ground-state Yb^+ .

Further, the values of K_0 and K_Z for the $^{171}\text{Yb}^+$ ground-state are recommended to be 31.0869(22) mHz/ μ T² and 14,010.78(49) Hz/ μ T, respectively, based on the calculated $g_J = 2.002615(70)$, $g'_J = -0.5377 \times 10^{-3}$ [61], and $A = 12,642,812,118$ Hz [19], as substituted into Eqs. (2) and (3). Within the QFS community, the prevailing values for K_0 and K_Z for the $^{171}\text{Yb}^+$ ground-state are 31.077 mHz/ μ T² and 14,008.6 Hz/ μ T, respectively [55]. However, the coefficients in Ref. [55] are derived using a non-relativistic g_J of 2.0023 (Nonrel.), which may underestimate the accuracy of the clock transition. The values reported in this work are consistent with the prevailing ones but offer improved reliability.

Assuming the B_0 value for our typical experimental

conditions is known precisely, the fractional SOZS $\delta\nu_{\text{SOZS}}$ caused by K_0 can be calculated to be

$$\begin{aligned} \delta\nu_{\text{SOZS}} &= \left| \frac{1}{A} \frac{\partial \Delta\nu_{\text{SOZS}}}{\partial K_0} \right| \delta K_0 = \left| \frac{B_0^2}{A} \right| \delta K_0 \\ &< 2 \times 10^{-18}, \end{aligned} \quad (10)$$

where we have used $B_0 = 0.1$ μ T under ideal experimental conditions [2], with $A = 12,642,812,118$ Hz [19], $K_0 = 31.0869$ mHz/ μ T², and $\delta K_0 = 0.0022$ mHz/ μ T² as the recommended values for the magnitude and uncertainty of K_0 , respectively, based on this work. Therefore, the uncertainty in K_0 will not impact the SOZS at a level that would compromise the accuracy of QFS operations at the 2×10^{-18} level, provided the applied magnetic field remains below the assumed value.

It is also imperative to calibrate the maximum level of fluctuation of B_0 . The uncertainty in the calibration of B_0 with respect to the K_Z is given by

$$\begin{aligned} \delta B_0 &= \left| \frac{\partial B_0}{\partial K_Z} \right| \delta K_Z = \left| \frac{\Delta\nu_L}{2K_Z^2} \right| \delta K_Z \\ &< 0.004 \text{ [nT]}, \end{aligned} \quad (11)$$

where we have used $\Delta\nu_L = 2.8$ kHz for $B_0 = 0.1$ nT under ideal experimental conditions [2], with $K_Z = 14,010.78$ Hz/ μ T and $\delta K_Z = 0.49$ Hz/ μ T representing the magnitude and uncertainty of K_Z , respectively, based on this work. Accordingly, the calibration of B_0 will be affected by the uncertainty in K_Z . Using our recommended K_Z value, the uncertainty in B_0 is expected to be less than 0.004 nT, which is sufficiently low to keep the uncertainty in the fractional SOZS relative to the clock frequency below 10^{-17} for the assumed magnetic field. The K_0 and K_Z factors determined in this work meet the accuracy requirements of state-of-the-art (1×10^{-14} [13]) and our anticipated (9×10^{-15} [19, 30]) microwave QFSs based on $^{171}\text{Yb}^+$ ions, supporting further advancements in such QFSs.

IV. CONCLUSION

In conclusion, we report the determination of the Landé g_J factor and Zeeman coefficients for the ground-state HFS of $^{171}\text{Yb}^+$. Systematic calculations of the g_J are performed using two independent methods: MCDHF and MRCl. These calculations yield consistent results, with a g_J factor of 2.002615(70), extending the consistency to the fifth decimal place. Based on this g_J factor, we derive precise values for the first- and second-order Zeeman coefficients, 14,010.78(49) Hz/ μ T and 31.0869(22) mHz/ μ T², respectively. The results presented here support the development of high-accuracy $^{171}\text{Yb}^+$ microwave QFSs and offer potential for improved constraints on variations in fundamental constants through frequency comparisons involving $^{171}\text{Yb}^+$ optical and hyperfine transitions, and advancing quantum computers based on trapped-ion.

ACKNOWLEDGMENTS

This work was supported by the National Key Research and Development Program of China (grant nos. 2021YFA1402100 and 2021YFB2801800), the National Natural Science Foundation of China (grant nos. 12474250 and 11874090) and the Space Application System of China Manned Space Program. We sincerely appreciate the efforts of the editor and the two reviewers in improving the quality of the manuscript.

J. H. and B. L. contributed equally to this work.

APPENDIX

The formula for calculating the weighted mean \bar{x} is

$$\bar{x} = \frac{\sum_{i=1}^n w_i x_i}{\sum_{i=1}^n w_i}, \quad (12)$$

where the weight $w_i = \frac{1}{(\delta x_i)^2}$, representing the weighting of each data point according to its uncertainty. The combined uncertainty of the weighted mean $\delta\bar{x}$ is calculated as,

$$\delta\bar{x} = \sqrt{\frac{1}{\sum_{i=1}^n w_i}}. \quad (13)$$

Substituting the MCDHF and MRCI calculation results, 2.002626(57) and 2.002604(55), respectively, the weighted mean result is 2.002615(40), where the number in parentheses indicates the weighted mean uncertainty.

-
- [1] B. L. Schmittberger and D. R. Scherer, arXiv preprint arXiv:2004.09987 (2020).
- [2] D. Berkeland, J. Miller, J. C. Bergquist, W. M. Itano, and D. J. Wineland, *Physical Review Letters* **80**, 2089 (1998).
- [3] E. Burt, J. Prestage, R. Tjoelker, D. Enzer, D. Kuang, D. Murphy, D. Robison, J. Seubert, R. Wang, and T. Ely, *Nature* **595**, 43 (2021).
- [4] U. Tanaka, H. Imajo, K. Hayasaka, R. Ohmukai, M. Watanabe, and S. Urabe, *Physical Review A* **53**, 3982 (1996).
- [5] B. Jelenković, S. Chung, J. Prestage, and L. Maleki, *Physical Review A* **74**, 022505 (2006).
- [6] J. Han, Y. Zuo, J. Zhang, and L. Wang, *The European Physical Journal D* **73**, 1 (2019).
- [7] J. Han, Y. Yu, B. Sahoo, J. Zhang, and L. Wang, *Physical Review A* **100**, 042508 (2019).
- [8] J. Han, H. Qin, N. Xin, Y. Yu, V. Dzuba, J. Zhang, and L. Wang, *Applied Physics Letters* **118** (2021).
- [9] J. Han, C. Pan, K. Zhang, X. Yang, S. Zhang, J. Berengut, S. Goriely, H. Wang, Y. Yu, J. Meng, *et al.*, *Physical Review Research* **4**, 033049 (2022).
- [10] J. Han, R. Si, H. Qin, N. Xin, Y. Chen, S. Miao, C. Chen, J. Zhang, and L. Wang, *Physical Review A* **106**, 012821 (2022).
- [11] H.-R. Qin, S.-N. Miao, J.-Z. Han, N.-C. Xin, Y.-T. Chen, J. Zhang, L. Wang, *et al.*, *Physical Review Applied* **18**, 024023 (2022).
- [12] S. J. Park, P. J. Manson, M. J. Wouters, R. B. Warrington, M. A. Lawn, and P. T. H. Fisk, 2007 IEEE International Frequency Control Symposium Joint with the 21st European Frequency and Time Forum , 613 (2007).
- [13] P. Phoonthong, M. Mizuno, K. Kido, and N. Shiga, *Applied Physics B* **117**, 673 (2014).
- [14] P. D. Schwindt, Y.-Y. Jau, H. L. Partner, D. K. Serkland, A. Ison, A. McCants, E. Winrow, J. Prestage, J. Kellogg, N. Yu, *et al.*, 2015 Joint Conference of the IEEE International Frequency Control Symposium & the European Frequency and Time Forum , 752 (2015).
- [15] P. D. Schwindt, Y.-Y. Jau, H. Partner, A. Casias, A. R. Wagner, M. Moorman, R. P. Manginell, J. R. Kellogg, and J. D. Prestage, *Review of Scientific Instruments* **87** (2016).
- [16] S. Mulholland, H. Klein, G. Barwood, S. Donnellan, P. Nisbet-Jones, G. Huang, G. Walsh, P. Baird, and P. Gill, *Review of Scientific Instruments* **90** (2019).
- [17] S. Mulholland, H. Klein, G. Barwood, S. Donnellan, D. Gentle, G. Huang, G. Walsh, P. Baird, and P. Gill, *Applied Physics B* **125**, 198 (2019).
- [18] J. Z. Han, Y. Zheng, S. N. Miao, Y. T. Chen, J. W. Zhang, L. J. Wang, L. Han, X. Chen, X. B. Xue, and S. K. Zhang, Joint Conference of the European Frequency and Time Forum and IEEE International Frequency Control Symposium (2023).
- [19] J. Han, N. Xin, J. Zhang, Y. Yu, J. Li, L. Qian, and L. Wang, *Applied Physics Letters* **125** (2024).
- [20] S. Miao, J. Zhang, H. Qin, N. Xin, J. Han, and L. Wang, *Optics Letters* **46**, 5882 (2021).
- [21] R. Warrington, P. Fisk, M. Wouters, and M. Lawn, *Frequency Standards and Metrology* , 297 (2002).
- [22] K. Hosaka, S. A. Webster, P. J. Blythe, A. Stannard, D. Beaton, H. S. Margolis, S. N. Lea, and P. Gill, *IEEE Transactions on Instrumentation and Measurement* **54**, 759 (2005).
- [23] T. Rosenband, D. Hume, P. Schmidt, C.-W. Chou, A. Brusch, L. Lorini, W. Oskay, R. E. Drullinger, T. M. Fortier, J. E. Stalnaker, *et al.*, *Science* **319**, 1808 (2008).
- [24] R. Godun, P. Nisbet-Jones, J. Jones, S. King, L. Johnson, H. Margolis, K. Szymaniec, S. Lea, K. Bongs, and P. Gill, *Physical Review Letters* **113**, 210801 (2014).
- [25] S. M. Brewer, J.-S. Chen, A. M. Hankin, E. R. Clements, C.-w. Chou, D. J. Wineland, D. B. Hume, and D. R. Leibrandt, *Physical Review Letters* **123**, 033201 (2019).
- [26] N. Stone, International Atomic Energy Agency (2019).
- [27] W. F. Meggers, *Journal of Research of the National Bureau of Standards. Section A, Physics and Chemistry* **71**, 396 (1967).

- [28] Y. Yu, B. Sahoo, and B. Suo, *Physical Review A* **102**, 062824 (2020).
- [29] G. Gossel, V. Dzuba, and V. Flambaum, *Physical Review A* **88**, 034501 (2013).
- [30] N. Xin, H. Qin, S. Miao, Y. Chen, Y. Zheng, J. Han, J. Zhang, and L. Wang, *Optics Express* **30**, 14574 (2022).
- [31] R. Lange, N. Huntemann, J. Rahm, C. Sanner, H. Shao, B. Lipphardt, C. Tamm, S. Weyers, and E. Peik, *Physical Review Letters* **126**, 011102 (2021).
- [32] M. Filzinger, S. Dörscher, R. Lange, J. Klose, M. Steinell, E. Benkler, E. Peik, C. Lisdat, and N. Huntemann, *Physical Review Letters* **130**, 253001 (2023).
- [33] V. Flambaum and A. Tedesco, *Physical Review C* **73**, 055501 (2006).
- [34] T. Dinh, A. Dunning, V. Dzuba, and V. Flambaum, *Physical Review A* **79**, 054102 (2009).
- [35] J. M. Pino, J. M. Dreiling, C. Figgatt, J. P. Gaebler, S. A. Moses, M. Allman, C. Baldwin, M. Foss-Feig, D. Hayes, K. Mayer, et al., *Nature* **592**, 209 (2021).
- [36] L. Feng, O. Katz, C. Haack, M. Maghrebi, A. V. Gorshkov, Z. Gong, M. Cetina, and C. Monroe, *Nature* **623**, 713 (2023).
- [37] S. A. Guo, Y. K. Wu, J. Ye, L. Zhang, W. Q. Lian, R. Yao, Y. Wang, R. Y. Yan, Y. J. Yi, Y. L. Xu, B. W. Li, Y. H. Hou, Y. Z. Xu, W. X. Guo, C. Zhang, B. X. Qi, Z. C. Zhou, L. He, and L. M. Duan, *Nature* **630**, 613 (2024).
- [38] M. Qiao, Z. Cai, Y. Wang, B. Du, N. Jin, W. Chen, P. Wang, C. Luan, E. Gao, X. Sun, H. Tian, J. Zhang, and K. Kim, *Nature Physics* **20**, 623 (2024).
- [39] W. M. Itano, *Journal of Research of the National Institute of Standards and Technology* **105**, 829 (2000).
- [40] M. Andersson and P. Jönsson, *Computer Physics Communications* **178**, 156 (2008).
- [41] K. Cheng and W. Childs, *Physical Review A* **31**, 2775 (1985).
- [42] P. Jönsson, M. Godefroid, G. Gaigalas, J. Ekman, J. Grumer, W. Li, J. Li, T. Brage, I. P. Grant, J. Bieroń, et al., *Atoms* **11**, 7 (2022).
- [43] P. Jönsson, G. Gaigalas, C. F. Fischer, J. Bieroń, I. P. Grant, T. Brage, J. Ekman, M. Godefroid, J. Grumer, J. Li, et al., *Atoms* **11**, 68 (2023).
- [44] F. Parpia and A. Mohanty, *Physical Review A* **46**, 3735 (1992).
- [45] I. P. Grant, *Relativistic quantum theory of atoms and molecules: theory and computation* (2007).
- [46] J. Li, P. Jönsson, M. Godefroid, C. Dong, and G. Gaigalas, *Physical Review A* **86**, 052523 (2012).
- [47] T. Zhang, L. Xie, J. Li, and Z. Lu, *Physical Review A* **96**, 012514 (2017).
- [48] S. Knecht, H. J. A. Jensen, and T. Fleig, *The Journal of Chemical Physics* **128** (2008).
- [49] H. J. A. Jensen, R. Bast, A. S. P. Gomes, T. Saue, L. Visscher, I. A. Aucar, V. Bakken, C. Chibueze, J. Creutzberg, K. G. Dyall, S. Dubillard, U. Ekström, E. Eliav, T. Enevoldsen, E. Faßhauer, T. Fleig, O. Fossgaard, L. Halbert, E. D. Hedegård, T. Helgaker, B. Helmich-Paris, J. Henriksson, M. van Horn, M. Iliáš, C. R. Jacob, S. Knecht, S. Komorovský, O. Kullie, J. K. Lærdahl, C. V. Larsen, Y. S. Lee, N. H. List, H. S. Nataraj, M. K. Nayak, P. Norman, G. Olejniczak, J. Olsen, J. M. H. Olsen, A. Papadopoulos, Y. C. Park, J. K. Pedersen, M. Pernpointner, J. V. Pototschnig, R. Di Remigio, M. Repiský, K. Ruud, P. Salek, B. Schimmelpennig, B. Senjean, A. Shee, J. Sikkema, A. Sunaga, A. J. Thorvaldsen, J. Thyssen, J. van Stralen, M. L. Vidal, S. Villaume, O. Visser, T. Winther, S. Yamamoto, and X. Yuan, (2022), 10.5281/zenodo.6010450, Please join our mailing list: <https://groups.google.com/g/dirac-users>.
- [50] A. S. Gomes, K. G. Dyall, and L. Visscher, *Theoretical Chemistry Accounts* **127**, 369 (2010).
- [51] M. Hubert and T. Fleig, *Physical Review A* **106**, 022817 (2022).
- [52] T. Fleig, J. Olsen, and C. M. Marian, *The Journal of Chemical Physics* **114**, 4775 (2001).
- [53] T. Fleig, J. Olsen, and L. Visscher, *The Journal of Chemical Physics* **119**, 2963 (2003).
- [54] T. Fleig, H. J. A. Jensen, J. Olsen, and L. Visscher, *The Journal of Chemical Physics* **124** (2006).
- [55] J. Vanier and C. Audoin, *The quantum physics of atomic frequency standards* (1989).
- [56] M. Safronova, M. Kozlov, and C. W. Clark, *Physical Review Letters* **107**, 143006 (2011).
- [57] M. A. Bohman, S. G. Porsev, D. B. Hume, D. R. Leibbrandt, and M. S. Safronova, *Physical Review A* **108**, 053120 (2023).
- [58] Z.-M. Tang, Y.-F. Wei, B. Sahoo, C.-B. Li, Y. Yang, Y. Zou, and X.-R. Huang, *Physical Review A* **110**, 043108 (2024).
- [59] B. Sahoo and P. Kumar, *Physical Review A* **96**, 012511 (2017).
- [60] D. K. Nandy and B. Sahoo, *Physical Review A* **90**, 050503 (2014).
- [61] N. Stone, *Atomic Data and Nuclear Data Tables* **111**, 1 (2016).